Article:
Tchio, J.A., Koskela, H., Adesanya, E. et al. (2026) Reaction kinetics of sulfate-activated slag: effects of activator type, slag source, and triisopropanolamine on electrical conductivity. Materials Advances. ISSN: 2633-5409

https://doi.org/10.1039/d6ma00554c

Materials Advances

ROYAL SOCIETY OF CHEMISTRY

PAPER

Published on 01 September 2026

Cite this: DOI: 10.1039/d6ma00554c

Reaction kinetics of sulfate-activated slag: effects of activator type, slag source, and triisopropanolamine on electrical conductivity

Julson Aymard Tchio,[ab] Hanna Koskela,[a] Elijah Adesanya,[a] Rafal Sliz,[c] Brant Walkley[b] and Juho Yliniemi*[a]

Electrical conductivity measurement using impedance spectroscopy is a promising technique for monitoring reaction processes in cementitious materials and understanding their reaction kinetics. In this study, alternating current electrochemical impedance spectroscopy (EIS), isothermal calorimetry, setting time measurements, compressive strength, zeta potential, and pore solution composition analysed *via* inductively coupled plasma optical emission spectroscopy (ICP-OES) were used to investigate the influence of calcium sulfate and sodium sulfate activators on the reaction mechanisms of two blast furnace slag (BFS) sources, with and without the addition of low concentrations of triisopropanolamine (TIPA). The results revealed that electrical conductivity trends varied significantly with both activator types and BFS reactivity. TIPA addition had a generally positive impact on strength development and demonstrated varying effects on conductivity depending on the BFS source and activator type. The findings confirmed that EIS is sufficiently sensitive to detect conductivity variations arising from different activator-BFS combinations and low dosage TIPA effects. However, the measured electrical conductivity was influenced not only by the ion concentrations in the pore solution but also by the reaction products, such as C-(A)-*S*-H and ettringite, as inferred from the combined trends of isothermal calorimetry, early strength and ICP-OES data, which are expected to progressively densify the microstructure and reduce pore network connectivity, thereby restricting ionic transport. This highlights the complex relationship between microstructure development and electrical properties in activated BFS systems.

Received 20th April 2026,
Accepted 16th August 2026

DOI: 10.1039/d6ma00554c

rsc.li/materials-advances

1. Introduction

Supplementary cementitious materials (SCMs) are by-products or natural materials that can partially replace Portland cement, thereby reducing clinker demand and CO_2 emissions. Alkali-activated materials (AAMs) are binders in which an aluminosilicate precursor, such as blast furnace slag (BFS), is activated by an alkaline or salt-based solution to form a hydrated binder without Portland cement (PC). PC production not only consumes substantial raw materials (such as limestone and clay) and calcination energy but also releases significant greenhouse gas emissions,[1,2] The most prevalent emission is CO_2,[3] with other highly polluting gases emitted into the atmosphere, including sulfur dioxide (SO_2) and nitrogen oxides (NO_x).[3] Growing environmental pressures have intensified the cement sector's challenge of balancing production demands with sustainability. Alkali-activated materials (AAMs), derived from industrial by-products like ground granulated blast furnace slag, present a viable pathway to minimise both energy consumption and emissions,[4,5]

AAM research has expanded considerably in recent years, with studies demonstrating that activator composition,[5] particle fineness and the chemical composition of blast furnace slag (BFS), which is high in CaO, SiO_2, and Al_2O_3 content relative to other SCMs such as fly ash and is widely available as a steel industry by-product, critically influence mechanical performance by promoting faster dissolution and reaction product formation,[4,6] Regarding activators, the use of sodium and potassium hydroxides or silicates has raised important concerns, notably the handling of viscous, corrosive, and hazardous solutions, thus limiting their industrial-scale applications[7–9] Furthermore, significant energy is required to produce sodium and potassium hydroxides or silicates, increasing the cost of the final

[a] *Fibre and Particle Engineering Research Unit, University of Oulu, P.O. Box 8000, FI 90014, Finland. E-mail: Juho.Yliniemi@oulu.fi*
[b] *School of Chemical, Materials, and Biological Engineering, University of Sheffield, UK*
[c] *Optoelectronics and Measurement Techniques Unit, University of Oulu, 90570, Oulu, Finland*

Table 1 Overview of activator types for alkali-activated BFS binders

Activator/ approach	Alkalinity	Key advantage	Key limitation	Industrial/research status	Ref.
NaOH/ Na-silicate	High	Fast reaction, high strength	Corrosive, hazardous, energy-intensive production	Widely researched; limited industrial-scale adoption due to handling/cost issues	7–11
Na_2CO_3	Moderate	Lower hazard than hydroxide/ silicate	Slower reactivity, carbonation-limited strength	Actively researched (including authors' prior work)	18,19
Na_2SO_4	Low	Low hazard, available industrial by-product route	Slower early-age reactivity, limited strength <3 days	Emerging research interest	12,15
$CaSO_4{\cdot}2H_2O$	Low	Low hazard, low cost, natural/by-product source (*e.g.*, FGD gypsum)	Very slow dissolution, low solubility limits ion release	Emerging/limited research	13–16
Organic ligand-modified systems	N/A (additive)	Improves early dissolution/ strength at low dosage	High dosage can be detrimental	Early-stage research	19–24

product. This is compounded by the fact that these strong alkaline solutions are neither naturally occurring nor industrial by-products, resulting in a substantial environmental impact during their manufacturing process. For example, soluble silicate production involves melting primarily sand and sodium carbonate at temperatures ranging from 1200 to 1400 °C to promote fusion, followed by dissolution in an autoclave with an appropriate steam pressure applied at temperatures ranging from 140 to 160 °C,[10,11]

For these reasons, there is growing interest in developing alternative activators for BFS, including sodium sulfate (Na_2SO_4)[12] and calcium sulfate ($CaSO_4{\cdot}2H_2O$),[13] which offer lower alkalinity and fewer hazards than hydroxide and silicate solutions. Furthermore, $CaSO_4$ can be sourced from industrial by-products such as FGD gypsum,[14] offering a cost-effective and sustainable route despite slower early-age reactivity, as detailed in Table 1. Sulfate-activated BFS binders are of industrial interest as a lower-cost, lower-hazard alternative to hydroxide/ silicate activation, offering a more scalable route to low-carbon binders, provided that their slower early-age reactivity can be mitigated. However, BFS activated with low-alkalinity activators is characterized by major challenges, including prolonged setting times and reduced mechanical properties during the first 24 hours or even the first 3 days of the reaction.[15] These activators influence the development of microstructure as well as physico-mechanical properties. Similarly, BFS reactivity plays a crucial role in the development of the microstructural properties of AAMs[15–17] The reaction products formed during the activation of BFS with sodium sulfate and calcium sulfate include calcium aluminum silicate hydrate (C-A-*S*-H) gels with a tobermorite-type structure, ettringite, gypsum and in some cases, monosulfate,[4,13,15,16,18] Seemingly small changes in the BFS composition also affect binder formation. For example, a generally high content of Mg or Ca leads to faster dissolution and, consequently, promotes microstructure formation in Na_2CO_3-activated BFS[18] and sodium silicate-activated BFS.[19]

Various measures have been implemented to improve the mechanical performance and dissolution rate of cementitious materials, including the addition of accelerating chemical admixtures. These admixtures enhance the reaction and accelerate setting, providing improved workability and higher mechanical strength. Recent studies have incorporated organic ligands as chemical admixtures, which at low dosages can significantly affect the dissolution of amorphous aluminosilicates and microstructural development. Tchio *et al.*[20] and Ramaswamy *et al.*[21] have shown that 0.1% additions of various organic ligands accelerate ion dissolution in Na_2CO_3-activated blast furnace slag *via* complexation mechanisms. Catecholate-based ligands, such as 2,3-dihydroxynaphthalene, complex Si, Ti, Ca, Mg, and Al ions. Phenolic compounds like 3,4-dihydroxybenzoic acid form soluble complexes with Fe, Ca, and Al.[22] Alkanolamine compounds (triethanolamine and triisopropanolamine) complex Ca and Mg ions, while tetrapotassium pyrophosphate similarly targets Ca and Mg,[23,24] This enhancement is attributed to the complexation ability of these ligands, which increases aluminosilicate dissolution from BFS[20–22] simultaneously resulting in improved mechanical properties. However, a high dosage of ligands (tetrapotassium pyrophosphate and 2,3-dihydroxynaphthalene)[21] negatively influences the strength in the early age. These observations are consistent with literature data from Portland cement systems, where the addition of ligands such as triethanolamine and triisopropanolamine has provided insights into the impact of ligands on reaction product development, ion concentration in the interstitial pore solution, and pore network evolution with respect to mechanical properties,[24–26] However, an understanding of the process of BFS activation with sodium sulfate, calcium sulfate, and ligands remains incomplete. Therefore, the implementation of advanced characterization techniques beyond conventional methods, such as isothermal calorimetry, setting time measurements, and X-ray diffraction, is essential.

Electrochemical impedance spectroscopy (EIS) has been widely used to characterize cementitious materials. Unlike calorimetry or setting time, which report a single bulk signal at limited ages, EIS enables continuous, real-time monitoring of ionic mobility and pore evolution throughout hydration, which is valuable for applications such as on-site or precast quality control.[27–29] This characterization technique involves applying an alternating current across a well-defined frequency range in fresh or hardened cement paste and provides information on the microstructural state and ionic mobility in the interstitial pore solution.[20,28,30] In this type of characterization, the cement paste is modelled as an electrical circuit, where the material's impedance is

represented by ohmic variations. For instance, Chi *et al.*[31] demonstrated that this technique can evaluate the impact of additives such as ethylenediaminetetraacetic acid (EDTA) at low concentrations during Portland cement hydration and provide information on the pore network development. Similarly, Sosa Gallardo *et al.*[28] showed that numerous physical and chemical changes can be detected during the first 24 h of the Portland cement reaction. Applying the same methodology, we evaluated the reactivity of different BFS sources of Na_2CO_3-activated BFS binders.[20] High-frequency resistance of the Na_2CO_3-activated BFS paste is related to its microstructure and ion mobility. Although this characterization technique has been used to investigate Na_2CO_3-activated BFS, the use of alkaline solutions with lower alkalinity, such as sodium sulfate (SS) or calcium sulfate (CS), fundamentally alters the system characteristics, including reaction kinetics, microstructural evolution, and reaction products formed. EIS studies on alkali-activated BFS have focused mainly on high-alkalinity hydroxide-, silicate-, or Na_2CO_3-activated systems. Their applicability to lower-alkalinity sulfate-activated systems (Na_2SO_4 and $CaSO_4$), which are of growing interest owing to their reduced hazard and cost, remains unestablished, representing a gap that this study addresses.

The objective of this study is therefore to further investigate the applicability of electrochemical impedance spectroscopy for alternative cementitious systems. Here, the electrical conductivity of sodium sulfate- and calcium sulfate-activated BFS from two different sources, along with the effect of TIPA on the hardening process, is investigated. Furthermore, isothermal calorimetry, setting time measurements, and pore solution analysis *via* inductively coupled plasma optical emission spectroscopy (ICP-OES) complement this investigation.

2. Materials and methods

2.1. Materials

The experiments were conducted using two types of BFS: one sourced from Japan (BFS-Jp) and the other from Finland (BFS-Fi). Their distinct chemical compositions are reported in our previous studies and shown in Table 2.[20] The LOI (loss on ignition at 950 °C) values were determined by thermogravimetry. The particle size distribution (PSD) of each slag, as shown in Fig. 1, was measured using a Beckman Coulter LS 13320 particle size analyzer. The D_{10}, D_{50}, and D_{90} values differ between the two slags: BFS-Fi (D_{10} = 1.4 μm, D_{50} = 11.5 μm, and D_{90} = 30.1 μm) and BFS-Jp (D_{10} = 1.2 μm, D_{50} = 9.1 μm, and D_{90} = 29.1 μm). The fineness and PSD of the slag are among the factors influencing its reactivity. BFS-Fi exhibits a coarser particle size distribution than BFS-Jp, which is consistent with a lower fraction of fine particles.

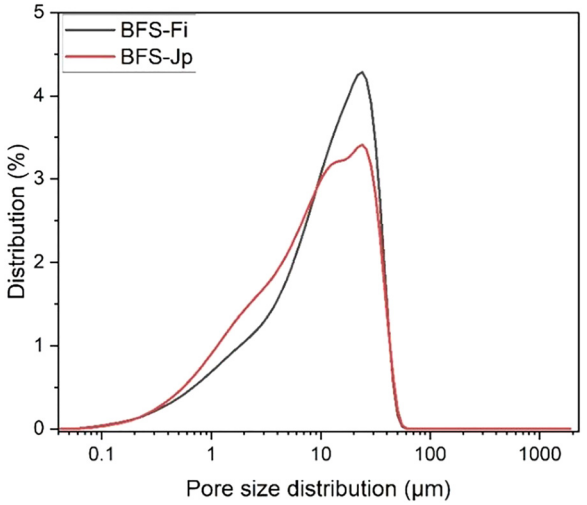

Fig. 1 Particle size distribution of different BFS samples.

2.2. Chemicals and organic ligands

Reagent-grade sodium sulfate (Na_2SO_4 ≥99% purity: Sigma-Aldrich, Belgium) and calcium sulfate (Ca_2SO_4 ≥98% purity: VWR, France) were used in this study. Both sulfates were supplied in anhydrous form, and their oxide-equivalent compositions (*i.e.*, SO_3 and CaO contents) followed the manufacturers' specifications provided in their certificates of analysis. The organic ligand used is triisopropanolamine (TIPA, ≥99% purity, Sigma-Aldrich, USA), an alkanolamine additive commonly employed as a grinding aid and hydration modifier for Portland cement. TIPA was selected following a preliminary screening of several candidate admixtures, based on its ability to accelerate the main exothermic hydration peak and enhance the early-age compressive strength in the BFS-Fi system, as reported in the Appendix.

2.3. Preparation of specimens

In this study, sodium sulfate (SS) and calcium sulfate (CS) were dissolved in deionized water at 40 °C and cooled to room temperature (21 ± 3 °C) before use. The selection of 40 °C is based on recent studies showing that this temperature allows enhanced solubility and ensures the complete dissolution of potential sodium sulfate decahydrate and calcium sulfate anhydrite.[32] SS- and CS-activated BFS were prepared with an activator dosage of 6 g per 100 g of the BFS precursor at a solution-to-binder ratio of 0.4, as detailed in Table 3. The activator dosage of 6 g per 100 g of the BFS precursor was selected based on values reported in the literature for Na_2SO_4 activation of slag-based binders.[15] The same mass dosage was applied to $CaSO_4$ to enable a direct understanding between the

Table 2 Chemical composition of BFS samples as analysed in ref. 19

Oxides (%)	MgO	Al_2O_3	SiO_2	SO_3	Na_2O	K_2O	CaO	TiO_2	MnO	Fe_2O_3	LOI
BFS-Fi	12.3	13.2	34.1	1.9	0.5	0.7	36.5	2.0	0.3	0.5	−2.3
BFS-Jp	5.2	13.1	33.5	0.6	0.18	0.2	43.4	0.5	0.1	0.4	−1.1

Table 3 Mix design for sulfate-activated slag systems with TIPA containing Na_2SO_4 fully dissolved under these conditions (nominal 1 M) and $CaSO_4$ partially dissolved due to its low aqueous solubility ($\sim$2 g L^{-1}), with the residue present as an undissolved solid phase

BFS source	Activator type	BFS (g)	Activator (g)	TIPA dosage (%)	w/s ratio	Sample code
BFS-Fi	Na_2SO_4	100	6	0.00	0.4	BFS-Fi-SS
		100	6	0.01, 0.05	0.4	BFS-Fi SS-TIPA-0.01; BFS-Fi SS-TIPA-0.05
BFS-Fi	$CaSO_4$	100	6	0.00	0.4	BFS-Fi CS
		100	6	0.01, 0.05	0.4	BFS-Fi CS-TIPA-0.01; BFS-Fi CS-TIPA-0.05
BFS-Jp	Na_2SO_4	100	6	0.00	0.4	BFS-Jp-SS
		100	6	0.01, 0.05	0.4	BFS-Jp SS-TIPA-0.01; BFS-Jp SS-TIPA-0.05
BFS-Jp	$CaSO_4$	100	6	0.00	0.4	BFS-Jp CS
		100	6	0.01, 0.05	0.4	BFS-Jp CS-TIPA-0.01; BFS-Jp CS-TIPA-0.05

two sulfate sources on a dosage-matched rather than equal dissolved-concentration basis, allowing the influence of sulfate ion availability and release rate (complete release from soluble Na_2SO_4 *versus* slow, solubility-limited release from $CaSO_4$) to be assessed with respect to the activated reaction. Dosages of 0.01% and 0.05% by mass of BFS of TIPA were incorporated based on earlier studies to observe their influence on the dissolution and microstructure of the SS- and CS-activated BFS. A mechanical mixer was used to combine the components for 3 min to form a homogeneous paste of the activated BFS. For compressive strength determination, the specimens were cast into stainless steel molds (2 cm $\times$ 2 cm), covered with a plastic film and demolded after 24 h of curing. After demolding, the specimens were cured under ambient conditions (sealed in a plastic bag and cured at 21 $\pm$ 3 °C) until testing at 1, 3, 7, 14, and 28 days.

2.4. Test methods

2.4.1. Setting time and compressive strength. To determine the initial and final setting times, 86 penetrations were applied during the first 15 h after mixing using the Vicatronic apparatus (Matest, E044N) by adapting the EN 196-3 standard due to different water/binder ratios and room humidity. Compressive strength tests were carried out using a calibrated Zwick/Roell (Z100) machine with a maximum load of 100 kN and a loading capacity at a constant displacement rate of 1.8 mm min^{-1}. Four different samples were used with a 2 $\times$ 2 $\times$ 2 cm specimen, and the average strength was reported.

2.4.2. Reaction kinetics. An 8-channel TAM Air isothermal calorimeter (TA Instruments) was used to analyze heat evolution for the first five days of hardening. The tests were performed at 20 °C. The specimens were maintained in plastic ampoule holders, and deionized water served as the reference. Prior to placement in the plastic ampoules and insertion into the calorimeter, the specimens were mixed for three minutes at 800–1000 rpm using IKA Eurostar Power control-viscosity stirrers. The reported results were normalized to the total mass of the fresh paste for each specimen. Due to *ex situ* sample mixing, the initial 45 minutes of recorded hydration data from the calorimeter were excluded from analysis.

2.4.3. Zeta potential. For zeta potential analysis, a 1% (w/v) suspension was prepared by dispersing 0.1 g of BFS powder in 10 mL of either 1 M sodium sulfate or calcium sulfate solutions, each prepared at a dosage of 6 g per 100 g of the BFS precursor (solution-to-binder ratio = 0.4). Under these conditions, Na_2SO_4 was fully dissolved (nominal concentration $\sim$1 M), whereas $CaSO_4$ was only partially dissolved due to its limited aqueous solubility, with the residue present as an undissolved solid phase. TIPA was added at the designated dosage (when applicable), and the mixture was stirred for approximately 45–60 minutes to ensure homogenization of the solution, BFS powder, and admixture. Following the mixing period, 2 mL of the suspension was extracted using a syringe for zeta potential measurements. The suspension was then transferred to disposable folded capillary cuvettes made of polycarbonate (DTS 1070). Zeta potential measurements were conducted using a Zetasizer Pro Blue instrument (ZSU5800 model, Malvern Panalytical, UK) equipped with ZS Explorer software. The measurements were performed at 22 °C, with an equilibration period of 60 s and a 30 s pause between each measurement. Three measurements were taken for each sample, and the median value was reported.

2.4.4. Electrical conductivity. The electrical conductivity of the pastes was measured using an electrochemical impedance spectroscopy (EIS) device (VIONIC powered by INTELLO, Metrohm Autolab). An 80 g portion of the freshly mixed paste was transferred into a custom-designed cell, as described in our previous study,[20] for impedance spectroscopy measurements. The paste was cast into a cylindrical 3 $\times$ 6 mm plastic mold with stainless steel electrodes embedded on both sides.[20,33] Measurements were taken at intervals starting from 15 minutes, then every 30 minutes up to 1.5 h, followed by hourly measurements until 11.5 h, covering the first 24 h. Subsequent measurements were conducted at 3, 7, and 28 days. The frequency range was 1 MHz to 100 Hz, with a sinusoidal amplitude of 0.1 V. Before testing at each frequency, the impedance of the cell in a short-circuit configuration without a specimen was measured to minimize the parasitic effects related to the cell components and leads. Using EIS measurements to fit the impedance response at the high-frequency arc of the Nyquist plot, the equivalent circuit model described and illustrated in Appendix[20] was employed, and the model parameters were used to determine the bulk resistance.[6,23] The choice of the Rs((RpCPE)CPE) circuit was based on its accuracy in simulating the responses of the $NaCO_3$-activated BFS paste to alternative current. Conductivity values were calculated from the resistivity values of each cementitious paste *via* the division of the cell constant by the bulk resistance, where the cell constant was obtained by measuring different concentrations of

activating solutions with known conductivities. The bulk resistance was considered the sum of the liquid and solid resistances Rs and the liquid–solid interface resistance Rp, and CPE represents the constant phase element of the paste.[20]

2.4.5. Pore solution extraction. Inductively coupled plasma optical emission spectroscopy (ICP-OES) was used to determine the pore solution composition extracted from the sodium sulfate-activated BFS pastes. The pore solution was extracted at different ages (1 h, 9.5 h, and 33.5 h (1 day 9 h) of the reaction) using an Instron 3000 universal testing machine. A titanium cylinder with an inner diameter of 6.5 cm, outer diameter of 16 cm, and a height of 28 cm was used. The pore solution was extracted under a loading of 400 MPa at a rate of 1 kN s^{-1} and then filtered using a 0.22 μm filter to ensure that only the liquid phase was analyzed. Prior to ICP-OES analysis, the extracted pore solutions were acidified to maintain a pH below 2 and prevent analyte precipitation. Acidification was performed by mixing 3 mL of the pore solution with 9 mL of a 6% nitric acid solution, yielding a 1 : 3 sample-to-acid ratio. The ion concentrations were corrected for the resulting dilution factor of 4.

3. Results

3.1. Setting time and compressive strength

For each BFS source and activator combination, the sample without TIPA addition serves as the reference, against which the effect of TIPA addition is compared. The penetration depth over time, along with the initial and final setting times of the pastes, are represented in Fig. 2. The setting time is observed to vary based on the early reactivity of BFS and the alkali activator used. The use of CS to activate the BFS samples (Fig. 2a) consistently prolongs both the initial and final setting times, while the SS-activated BFS sample (Fig. 2b) appears to have an earlier effect on the first penetration. The effect of TIPA on setting behavior varied between BFS sources, and the summary table is represented in the appendix (Table A). With BFS-Jp, TIPA dosage accelerated both the initial and final setting times, while with BFS-Fi, the most significant acceleration of the setting times occurred at a 0.05% TIPA addition. BFS reactivity is influenced by the glass structure and its capacity to dissolve ions, particularly in sulfate-activated cementitious systems.[34] At this stage, it can be assumed that the prolonged setting time for BFS-Fi is related to the low precipitation of the reaction products compared to BFS-Jp.

The compressive strength results are presented in Fig. 3, illustrating the influence of the SS and CS activators and TIPA on the strength development of the activated BFS at ages of 1, 3, 7, 14, and 28 days. The final setting time marks the consolidation of the sample, inhibiting the penetration of the Vicat needle rather than strength development. BFS-Fi samples did not harden during the first 3 days, regardless of the activator type (SS or CS) or TIPA addition, except for BFS-Fi SS-TIPA 0.01%, which exhibited a compressive strength of 0.6 MPa at 1 day. At 3 days, an increase to 15 MPa with SS and 8 MPa with CS is observed, and this strength development is more pronounced with TIPA addition. BFS-Fi-CS exhibited the second-highest strength development from 7 to 28 days, while BFS-Fi-SS achieved lower strength. TIPA addition showed beneficial effects: the 28 day strength of BFS-Fi-SS improved with TIPA, while BFS-Fi-CS demonstrated a significant strength increase at 0.01% TIPA concentration, despite its low strength at 14 days compared to the reference. This contrasting behavior suggests that the ligand initially delays microstructure evolution, but with time the microstructure becomes denser. This indicates that TIPA first acts as a temporary inhibitor and later as a hydration promoter, although further increases in TIPA dosage result in decreased 28 day strength. In contrast, with BFS-Jp, a compressive strength of 13 MPa is achieved with SS after 1 day of hardening, and it increases up to 33 MPa after 3 days. TIPA causes a minor decrease in 1 day and 3 days strengths in the SS-activated BFS-Jp sample. CS-activated BFS-Jp has low 1 day compressive strength (0.7 MPa); however, TIPA increases it up to 6 MPa. After 3 days, the strength increased to 20 MPa with and without TIPA.

These results are in line with setting time measurements, which also demonstrated the prolonged microstructure development period of BFS-Fi. From 7 to 28 days, BFS-Jp-SS demonstrated the greatest strength development among all systems,

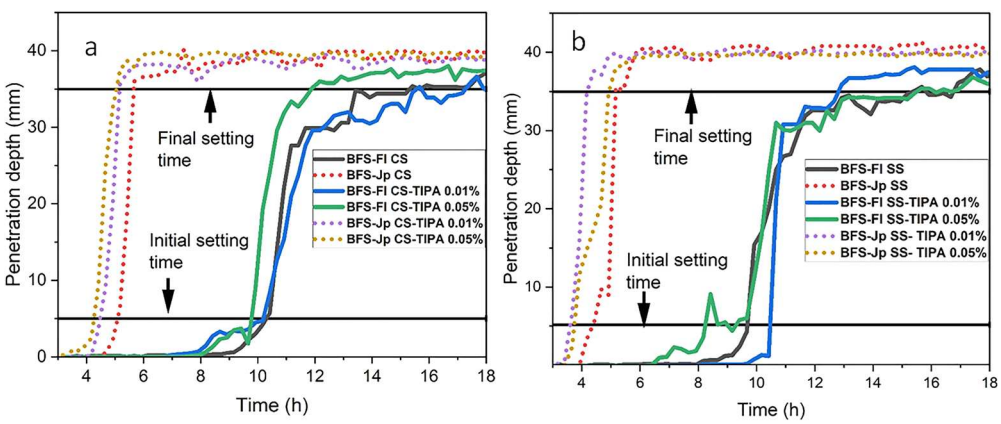

Fig. 2 Setting times of CS (a) and SS (b) -activated BFS.

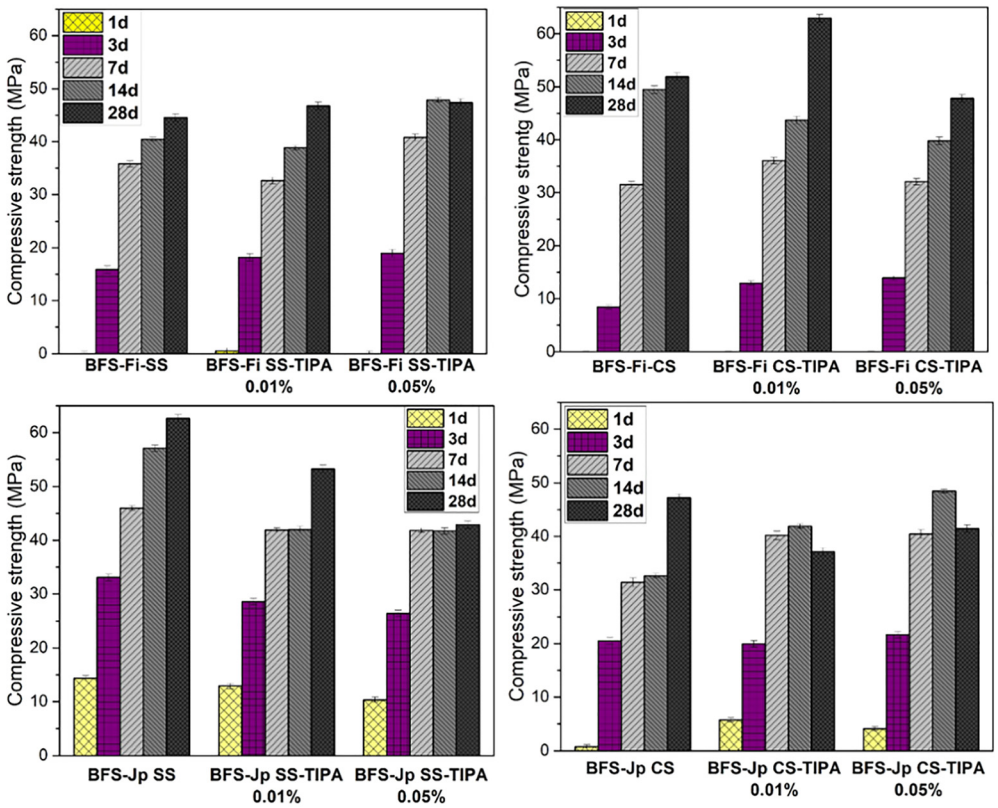

Fig. 3 Compressive strengths of SS- and CS-activated BFS with and without TIPA.

while BFS-Jp-CS presented marginally slower strength development between 7 and 14 days, before showing a 10% improvement at 28 days but achieving higher strength than BFS-Fi-SS at the same curing ages. However, TIPA addition leads to a decrease in strength in both the BFS-Jp-SS and BFS-Jp-CS systems, indicating a detrimental effect on the reaction kinetics.

3.2. Isothermal calorimetry

Isothermal calorimetry results of the samples are illustrated in Fig. 4. In BFS-Fi systems, the reaction behavior differs significantly depending on the activator type and TIPA addition. In CS-activated BFS-Fi, the addition of TIPA prolongs the main exothermic peak of the reaction from 50 to 60 h, indicating a retarding effect on the reaction kinetics. Meanwhile, in SS-activated BFS-Fi, the main exothermic peak occurs earlier, around 40–45 h, with a higher heat flow intensity compared to the CS system. These results demonstrate that both the activator type and TIPA presence influence the reaction rate and heat evolution in the slag.

In contrast, the BFS-Jp systems exhibited markedly faster reactivity with induction periods of less than 1 h in both SS- and CS-activated samples. In the CS-activated BFS-Jp sample, the reaction kinetics reveal two distinct exothermic peaks: the first at 6 h and the second between 40 and 45 h. A similar dual-peak behavior was observed in the SS-activated BFS-Jp sample, with the first early exothermic peak at 4 h and the second main exothermic peak at 15 h. One unexpected observation with the addition of TIPA to SS-activated BFS-Jp is an apparent endothermic reaction occurring after 45 h of curing. Repeating the experiments with a different calorimeter confirmed that this response is reproducible and intrinsic, though its cause requires further investigation.

The variation in the heat release patterns between BFS-Fi and BFS-Jp, as observed in Fig. 5, suggests that differences in the BFS source result in different reaction mechanisms upon using SS or CS activators and with the incorporation of TIPA. However, it is important to note that cumulative heat does not necessarily correspond to higher structural performance.

3.3. Zeta potential

The zeta potential measurements of BFS-Fi and BFS-Jp are presented in Fig. 6. These measurements were performed to evaluate how the sulfate activator and TIPA influence the surface charge of the BFS particles, rather than to characterize the activator solutions themselves. It should be noted that, due to its limited aqueous solubility, $CaSO_4$ was not fully dissolved under the tested conditions; the BFS particles in the CS suspensions were therefore in contact with a saturated Ca/SO_4 solution together with residual undissolved $CaSO_4$, in contrast to the fully dissolved Na_2SO_4 (SS) system. As shown in Fig. 6, BFS-Fi generally had a more negative zeta potential than BFS-Jp, indicating a different surface charge environment (possibly due to composition or prehydration differences.[35,36]

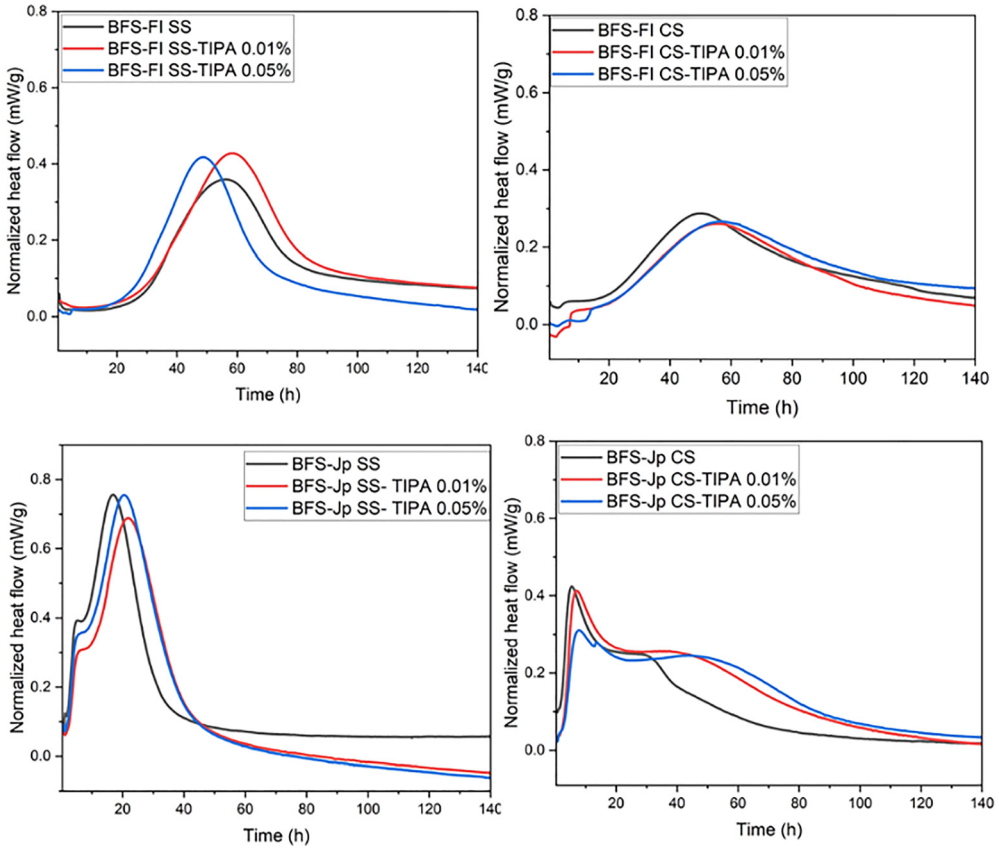

Fig. 4 Heat flow of the SS- and CS-activated BFS pastes with and without TIPA.

Adding TIPA made the zeta potential less negative in all cases, but the effect was much more pronounced for BFS-Jp (in both SS and CS solutions) than for BFS-Fi. A less negative (*i.e.*, higher) zeta potential implies that TIPA is neutralizing some of the surface charge,[37] suggesting a stronger adsorption or interaction of TIPA with BFS-Jp particles. This difference implies that the ligand's effect is surface-chemistry-dependent.

3.4. Electrical conductivity

The electrical conductivity measurement results are shown in Fig. 7. For the SS- and CS-activated BFS-Fi samples, the electrical conductivity remains constant from 15 min to approximately 11.5 h, indicating that BFS-Fi does not react when mixed with SS or CS activators, which correlates with the long setting time and isothermal calorimetry. A standard deviation of 0.015 ± 0.001 S cm^{-1} was noted in electrical conductivity;[20] however, in the early stages of the reaction, conductivity is mainly influenced by the activator type. The 18-fold lower conductivity of CS-activated BFS-Fi and BFS-Jp compared to SS-activated BFS-Fi and BFS-Jp may be attributed to the inherent solution properties of the activators. As Na ions have higher mobility compared to Ca ions, the SS-activated systems have higher conductivity than the CS-activated ones. The CS solution exhibited a pH of 10.36 and a conductivity of 0.285 S m^{-1}, while the SS solution showed a pH of 7.34 and a conductivity of 8.77 S m^{-1} (measured using a conductivity meter).[38] Moreover, the higher concentration of Ca ions in the pore solution may exert a strong inhibiting effect on slag dissolution and also inhibit Ca dissolution from BFS due to the common ion effect, which aligns with the work of Zhai *et al.*[39] who studied calcium hydroxide-activated BFS.

BFS-Fi samples with both activators exhibit relatively constant conductivity up to approximately 33 h before a progressive decrease until 28 days. This delayed reaction correlates with the longer setting times observed in Fig. 2. The decrease in electrical conductivity marks the formation of reaction products, as the growth of phases leads to microstructural development and densification.

Low dosage of TIPA influences electrical conductivity in all systems. For instance, in SS-activated BFS-Fi with TIPA, the conductivity decreases during the first 3 days of the reaction compared to the reference, while in BFS-Fi CS containing TIPA, a complex trend is observed depending on the dosage. TIPA increases conductivity during the 1-to-3-day range, which aligns with better strength development in those samples. In contrast, CS-activated BFS-Jp with TIPA demonstrated an increase in conductivity during the first 6 h, then a progressive decrease for 3 days, and this phenomena correlates with the early age strength measured for those samples. The more pronounced reactivity of TIPA with BFS-Jp relative to BFS-Fi can be partly explained by their basicity moduli. BFS-Jp exhibits higher CaO/SiO_2 (1.29) and CaO + MgO/SiO_2 (1.45) ratios than BFS-Fi

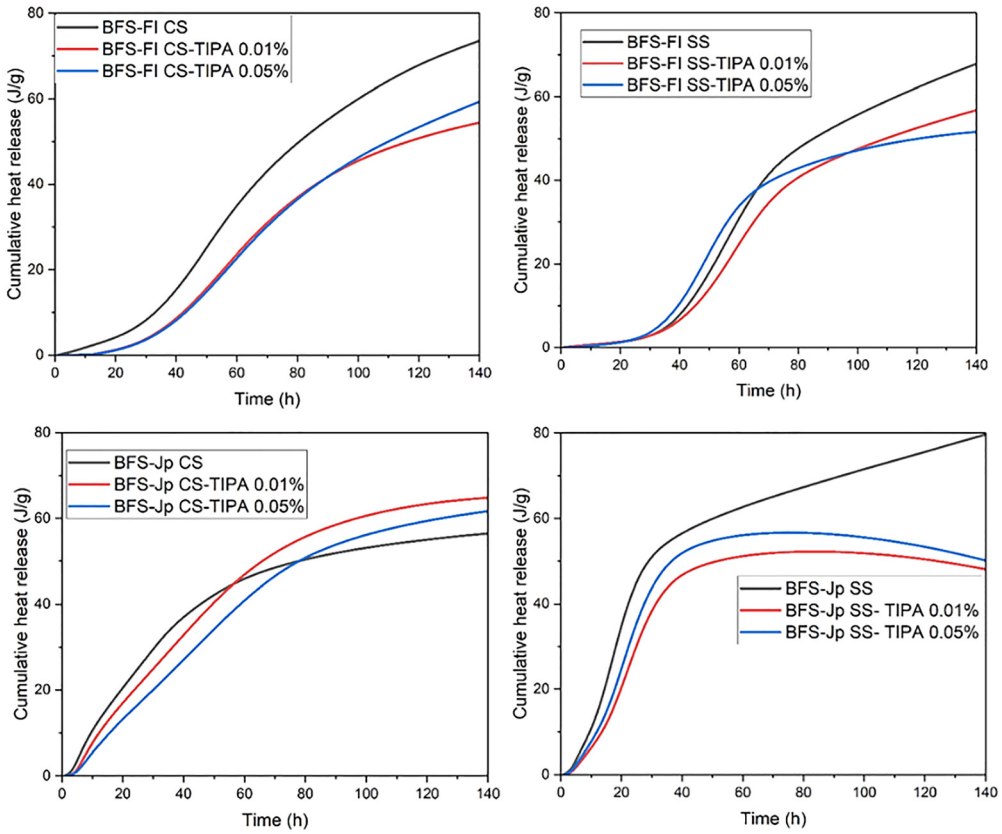

Fig. 5 Cumulative heat release of the SS- and CS-activated BFS pastes with and without TIPA.

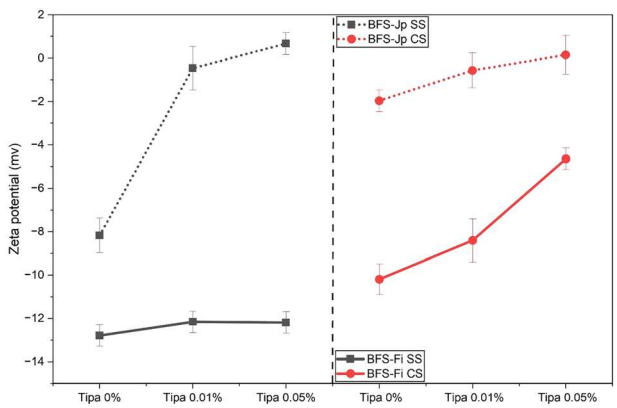

Fig. 6 Zeta potential of the paste suspensions.

(1.07 and 1.43, respectively), which is generally associated with a less polymerized aluminosilicate glass network, facilitating dissolution. This further supports the enhanced conductivity behavior observed in BFS-Jp.

3.5. Pore solution extraction

Pore solution extraction was performed for the SS-activated samples (Fig. 8). Sulfur and sodium concentrations are provided in the Appendix given that these concentrations are much higher than those of other ions. During the first hour, the ion concentrations were higher in the pore solution, with Ca as the major ion. TIPA addition increased the Ca concentration in the BFS-Fi sample, whereas in BFS-Jp, TIPA increased the Al, Si, and Mg concentrations. The varying effect of TIPA on the pore solution composition shows the complex and unknown dissolution-complexation-precipitation reactions occurring in cement systems.

As the hardening reactions proceed, a sharp drop in ion concentrations occurs in both BFS samples. TIPA increased the ion concentrations in BFS-Jp, while mainly decreasing them in BFS-Fi (one exception is Al, which had a higher concentration with TIPA).

Regarding S and Na concentrations (Appendix), in general, their concentration decreased with time indicating their incorporation in the reaction products. TIPA had a varying, but clear, effect on time and the BFS source; at 9 h 30 min with BFS-Fi, increased concentrations were detected, whereas in the other samples, decreased concentrations were observed.

4. Discussion

The electrical conductivity of cementitious materials is commonly attributed to the ion concentration in the pore solution and charge transfer through the pore network.[20,29] However, several factors can influence electrical conductivity. The electrical conductivity in Fig. 7 shows that conductivity varies depending on the reaction kinetics of BFS, reaction product formation, and activator type. During the initial dissolution

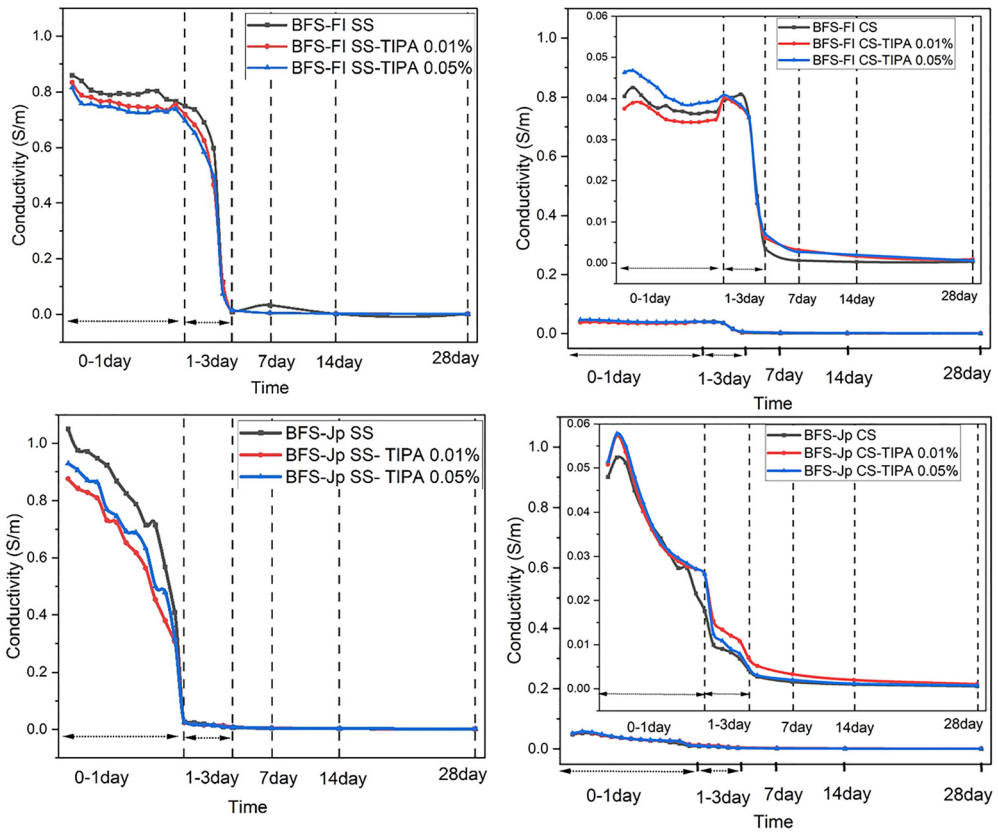

Fig. 7 Electrical conductivity of SS- and CS-activated BFS.

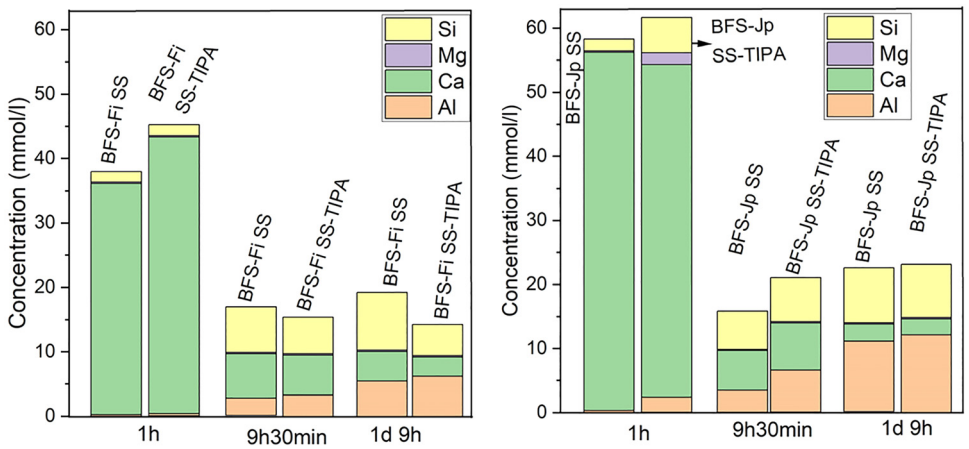

Fig. 8 Pore solution compositions of the SS-activated BFS samples.

(0–12 h), EIS shows ionic transport in the pore solution, as evidenced by the constant conductivity in the BFS-Fi systems. The SS activator maintains higher conductivity than CS due to the complete dissolution of Na_2SO_4 *versus* only 1.5% $CaSO_4$ dissolution. This establishes that the baseline ionic mobility is dominated by the activator chemistry rather than the slag reaction. During percolation (12–48 h), EIS detects solid network formation marked by decline in conductivity correlating with calorimetric peaks (*e.g.*, 32 h in BFS-Fi-SS). This stage occurs within hours for BFS-Jp. The lack of correlation between the ion concentration and conductivity demonstrates that EIS is sensitive to the microstructural topology rather than the ionic strength alone. For instance, BFS-Fi shows 0.6. S m^{-1} despite a lower ion concentration, while BFS-Jp exhibits 0.02 S m^{-1} with a higher concentration at 1 d 9 h. During product precipitation (2–7 days), EIS captures pore refinement as the reaction

products fill the capillary porosity. TIPA modifies this response by temporarily influencing the ion concentrations (Ca, Mg, and Al) and mobility. From 7 to 28 days, progressive conductivity reduction reflects microstructural maturation and densification, independent of ion concentration stabilization.

When BFS is activated with SS or CS, the hydroxyl ions (OH^-) are present in the activator solutions after the initial rapid proton-metal exchange reactions between water and BFS. Hydroxyl ions facilitate further depolymerization of the aluminosilicate network (–O–Al–O–Si–O–) bonds in the slag that are substituted by Ca and in some cases Mg is present in the structure. This leads to the dissolution of ions into the liquid phase, which participate in the formation of reaction products. Eventually, this leads to the formation of C-A-*S*-H as the main reaction product.[15] Furthermore, sulfate anions influence the precipitation reactions by forming other reaction products such as ettringite ($C_6AS_3H_{32}$),[16,18] potentially serving as nucleation sites that can influence C-A-*S*-H formation. The lower reactivity of BFS-Fi *vs.* BFS-Jp is attributed to possible pre-hydration based on the LOI[40] and its lower Ca content, as indicated in Table 1. The contrasting strength trends (CS > SS for BFS-Fi, but SS > CS for BFS-Jp) arise from the interplay between the slag pre-hydration state and activator dissolution kinetics. Specifically, the higher LOI of BFS-Fi (−2.2%) indicates that the pre-hydration is more effectively disrupted by the Ca-rich CS activator. This creates localized supersaturation at the slag-solution interface, whereas the fully dissolved SS activator lacks sufficient chemical driving force to penetrate the pre-hydrated layer (evidenced by the extended 33-h induction period and delayed 40–45 h exothermic peak). Conversely, the minimal pre-hydration (LOI: −1.1) and reactive glass structure of BFS-Jp (as demonstrated in R3 analysis in appendix) favor SS activation because complete sulfate dissolution provides continuous SO_4 for network depolymerization and higher Na mobility sustains steep concentration gradients driving dissolution, while CS activation suffers from the common ion effect, where saturated Ca inhibits further slag calcium release. This inhibition manifests as dual calorimetric peaks (at 6 hours for surface Ca and 40–45 h for bulk glass dissolution) and ultimately lowers strength despite early reaction product formation. The opposite TIPA effects at 0.05% dosage in the BFS-Jp systems accelerated the setting time in SS but retarded it in CS, resulting from the competitive TIPA and BFS interactions. In the CS-activated systems, TIPA may potentially influence Ca, Mg, and Al ions (evidenced by increased conductivity during the first 6 hours), temporarily preventing precipitation until TIPA consumption triggers burst precipitation (indicated by a conductivity drop and a second exothermic peak observed at 40–45 hours), whereas in the SS-activated systems, Na and SO_4 ions create a competing ionic environment where TIPA preferentially adsorbs onto slag surfaces (less negative zeta potential), forming steric barriers that influence the reaction kinetics.

Overall, low alkaline SS and CS can be used to activate BFS based on compressive strength development and isothermal calorimetry results. Activators themselves are quite different despite both being sulfates; Na_2SO_4 has much higher solubility than $CaSO_4$ which affects further dissolution and precipitation reactions. This, and the inherent lower mobility of Ca *vs.* Na, explains the 18 times lower electrical conductivity of the CS-activated samples compared to the SS-activated samples. When 6 g of powder is dissolved in 40 mL of distilled water at 40 °C (attempting 1.1 mol kg^{-1} target concentrations for both), Na_2SO_4 completely dissolves, forming a clear solution at 1.06 mol kg^{-1}. This value is well below its saturation limit of 6.81 mol kg^{-1} ($K_{sp} \approx 0.455$) with ions remaining largely dissociated due to weak pairing (γNa = 0.478 and γSO_4 = 0.013).[32] In contrast, $CaSO_4$ exhibits only 1.5% dissolution, reaching saturation at 0.017 mol kg^{-1} ($K_{sp} \approx 2.8 \times 10^{-5}$) with 98.5% remaining as a precipitate. This 400× solubility difference results from strong Ca–SO_4 association (γCa = γSO_4 = 0.312), which, combined with the low K_{sp} and lower Ca mobility, drives precipitation.[32]

TIPA addition modified the electrical response in each system depending on the BFS source, demonstrating that impedance spectroscopy can detect the impact of small ligand proportions. TIPA can complex ions such as Ca, Mg, and Al,[24,41] and thus promote the dissolution reaction, which was observed to some extension based on the pore solution compositions. However, the effect varied depending on the BFS source, demonstrating the complex overall relations between dissolution-complexation-precipitation reactions. Zeta potential measurements showed a more pronounced effect of TIPA with BFS-Jp, showing sensitive surface reactions depending on the BFS source. These types of interactions can modify the reaction kinetics through electrostatic and steric interactions resulting from surface and ion complexation, which eventually impact the mechanical properties. The difference suggests that microstructural development and pore network characteristics play a more significant role than the ion concentration alone. This establishes a relationship between electrical conductivity and calorimetry: calorimetry detects the exothermic reactions of cementitious phase formation, while impedance spectroscopy provides information on the microstructural evolution and ion mobility. To analyze the trends observed across the different characterization techniques, Table 4 provides a comparative summary of the setting time, compressive strength, calorimetry, zeta potential, and electrical conductivity results for each BFS source and activator combination, highlighting how the BFS source, activator type, and TIPA addition jointly govern the reaction behavior.

This study systematically correlates electrical conductivity with the complex chemical interactions of TIPA in low-alkalinity AAMs. EIS detects subtle modifications in the reaction kinetics induced by trace TIPA dosages (0.01–0.05%) across different slag sources and activator chemistries. The electrical conductivity evolution reflects not only the ionic concentration but also the intricate interplay of TIPA's influence on dissolution and precipitation phenomena, microstructural topology, and pore network percolation. This represents a multi-parameter response that conventional techniques such as isothermal calorimetry or compressive strength testing cannot independently resolve. By integrating EIS with zeta potential measurements, pore solution extraction, and calorimetry, this work demonstrates that

Table 4 Comparative summary of the setting time, strength, calorimetry, zeta potential, and conductivity trends (↑: increase and ↓: decrease)

Parameter	BFS-Fi-SS	BFS-Fi-CS	BFS-Jp-SS	BFS-Jp-CS
Setting time	Earlier first penetration	Prolonged (initial and final)	Accelerated with TIPA	Accelerated with TIPA
1 day strength	0 MPa (0.6 MPa at SS-TIPA 0.01%)	0 MPa	13 MPa	0.7 MPa (>6 MPa with TIPA)
3 day strength	15 MPa (↑ with TIPA)	8 MPa (↑ with TIPA)	33 MPa (slight ↓ with TIPA)	20 MPa (slight ↑ with TIPA)
28 day strength	Improved with TIPA	↑ significantly at 0.01% TIPA	Highest overall; ↓ with TIPA	↓ with TIPA
Main exothermic peak	40–45 h	445–60 h (extended with TIPA)	Dual peaks: 4 h and 15 h	Dual peaks: 6 h and 40–45 h
Induction period	Extended (20 h)	Extended (20 h)	<1 h	<1 h
Zeta potential (base)	More negative	More negative	Less negative	Less negative
Zeta potential (TIPA effect)	Less negative (mild)	Less negative (mild)	Less negative (pronounced)	Less negative (pronounced)
Electrical conductivity	Steady ↓ to 24 h, then steep ↓	18× lower than SS; steady ↓, then steep ↓	Rapid decline (early reaction)	↑ first 6 h (TIPA), then ↓. 18× lower than SS
Effect of TIPA on conductivity	↓ compared to the reference	↑ or ↓ with TIPA dosage 0–1 day, then ↑ 3–28 days compared to the reference	Rapid decline (early reaction) compared to the reference	↑ 0–6 h, then progressive ↓; ↑ compared to the reference

Activator solution properties: SS – pH 7.34, conductivity 8.77 S m^{-1} and CS – pH 10.36, conductivity 0.285 S m^{-1}.

TIPA's influence is surface-chemistry-dependent (as evidenced by differential zeta potential shifts between BFS-Fi and BFS-Jp) and activator-specific. These findings challenge the simplistic view of TIPA as a universal reaction kinetics accelerator. Instead, TIPA acts as a context-dependent modifier whose influence on chemical ions, surface adsorption, and steric effects competes dynamically with activator dissolution behavior and the slag pre-hydration state.

However, the study acknowledges significant limitations inherent to both the experimental methods and the fundamental complexity of the system; first, the mechanistic interpretation of the EIS data remains partially speculative because the technique cannot directly distinguish between the capacitive effects from C-A-*S*-H layer formation and frequency-dependent relaxation processes associated with adsorbed water or charged surface sites. This indicates that while conductivity trends correlate with calorimetric events and strength development, the physicochemical origin of each conductivity inflection point requires validation through complementary microstructural characterization. Second, the TIPA reaction pathways themselves are not fully elucidated although the pore solution data confirm the influence of TIPA ions (increased Ca, Al, and Mg concentrations with TIPA in BFS-Jp) and surface modification (zeta potential shifts). The study did not quantify the TIPA consumption kinetics, identify specific metal-TIPA complex stoichiometries (*e.g.*, Ca-TIPA *vs.* Al-TIPA stability constants at varying pH), or confirm whether TIPA is incorporated into solid phases (C-A-*S*-H interlayers or ettringite structures)[26] or degraded over time, leaving open questions about whether the observed "temporary inhibitor" effect results from reversible complexation, irreversible surface passivation, or time-dependent TIPA decomposition in alkaline environments. EIS as a multi-stage diagnostic tool in AAM systems categorizes early-age signals as activator-dominated ionic transport, mid-age signals as percolation-driven conductivity decline, and late-age signals as densification-controlled impedance evolution. This demonstrates that even when the exact chemical mechanisms remain incompletely resolved, EIS serves as a sensitive fingerprinting technique capable of detecting batch-to-batch variability (slag source effects), formulation changes (activator type, TIPA dosage), and reaction kinetics.

5. Conclusion

This study evaluated whether AC impedance spectroscopy (EIS) could distinguish the influence of calcium sulfate (CS) and sodium sulfate (SS) activators and TIPA addition on the reaction kinetics of two chemically distinct BFS sources (BFS-Fi and BFS-Jp). The main findings are summarized below:

• Activator solubility governs conductivity and reaction kinetics. CS-activated systems exhibited 18-fold lower conductivity, attributed to the low aqueous solubility of $CaSO_4$ (~1.5% dissolution *vs.* near-complete Na_2SO_4 dissolution). This was consistent with the slower, delayed heat release in CS-activated systems observed by calorimetry.

• The chemical composition of BFS directly influences its reactivity and the performance of the activator. BFS-Jp (higher CaO/SiO_2 = 1.29, $CaO + MgO/SiO_2$ = 1.45, and lower LOI = 1.1%) exhibited faster dissolution, earlier setting time, and higher early strength than BFS-Fi (CaO/SiO_2 = 1.07, $CaO + MgO/SiO_2$ = 1.43, and higher LOI = 2.3%, indicative of pre-hydration). This compositional difference explains why SS activation outperformed CS for BFS-Jp, while CS activation outperformed SS for BFS-Fi, demonstrating that the activator choice should be tailored to the slag reactivity/composition rather than applied universally.

• Electrical conductivity does not correlate directly with the pore solution ion concentration. Conductivity trends were instead governed by microstructural development and pore network

evolution, indicating that EIS captures physical percolation and densification processes beyond simple ionic strength.

• TIPA effects are reactivity-dependent and not universal. TIPA improved strength in the lower-reactivity BFS-Fi system while decreasing strength in the higher-reactivity BFS-Jp system, regardless of activator type, showing that ligand performance depends on the baseline reaction kinetics of the host system rather than acting as a uniform accelerator.

• EIS is a sensitive and complementary diagnostic tool. EIS successfully detected conductivity variations arising from the activator type, BFS source, and low-dosage (0.01–0.05%) and TIPA additions that would not be resolvable by calorimetry or strength testing alone, confirming its value for the real-time, non-destructive monitoring of reaction kinetics in low-alkalinity activated systems.

Based on these findings, the choice and dosage of both the activator and ligand should be guided by the specific chemical composition and inherent reactivity of the BFS source, rather than a one-size-fits-all approach; CS activation combined with TIPA is recommended for low-reactivity slags (BFS-Fi), whereas SS activation without TIPA is preferable for high-reactivity slags (BFS-Jp). This work provides a foundation for using EIS as a quality-control and monitoring tool for low-alkalinity, sulfate-activated slag binders in industrial and precast concrete applications, supporting the development of lower-hazard, lower-cost alternatives to conventional hydroxide/silicate activation. It also establishes a basis for tailoring admixture strategies to specific slag sources, which is relevant to industries seeking to valorize regionally variable slag by-products.

Author contributions

Julson Aymard Tchio: conceptualisation, investigation, data curation, formal analysis, methodology, validation, formal analysis, visualisation, writing – original draft, writing – review & editing. Hanna Koskela: investigation, data curation, formal analysis, visualisation. Elijah Adesanya: conceptualisation, resources, data curation, supervision, visualisation, writing – review & editing. Brant Walkley: data curation, supervision, visualisation, writing – review & editing. Rafal Sliz: data curation, validation, writing – review & editing. Juho Henrik Yliniemi: conceptualisation, data curation, resources, methodology, supervision, visualisation, writing – review & editing, funding acquisition, project administration.

Conflicts of interest

The authors declare that they have no known competing financial interests or personal relationships that could have appeared to influence the work reported in this paper.

Data availability

We have provided a link to access the research data: https://doi.org/10.23729/fd-86257ad3-e608-3f33-8f2d-8ec62170f71c.

Supplementary information (SI) is available. See DOI: https://doi.org/10.1039/d6ma00554c.

Acknowledgements

This work was co-funded by the European Union under the Marie Skłodowska-Curie Actions project I4WORLD (grant no. 101081280). However, the views and opinions expressed are those of the author(s) only and do not necessarily reflect those of the European Union or the European Research Executive Agency [REA]. Neither the European Union nor the REA can be held responsible for them. Yliniemi acknowledges the Research Council of Finland (grant #354263). Julson Tchio acknowledges the Tutkijat maailmalle grant system through the Walter Ahlström in foundation (20250042). Additionally, the authors would like to thank the Centre of Material Analysis (University of Oulu) and the lab technicians (FPERU, University of Oulu) for their support with the material characterisation techniques.

References

1 R. Amran, M. Makul, N. Fediuk, N. I. Lee, Y. H. Vatin, K. Lee and Y. Y. Mohammed, Global carbon recoverability experiences from the cement industry, *Case Stud. Constr. Mater.*, 2022, **17**(4), 01439, DOI: 10.1016/j.cscm.2022.e01439.

2 V. Sousa and J. A. Bogas, Comparison of energy consumption and carbon emissions from clinker and recycled cement production, *J. Cleaner Prod.*, 2021, **306**(4), 1–13, DOI: 10.1016/j.jclepro.2021.127277.

3 A. B. Mlitan, *Cement Dust Pollution and Environment BT – Toxicology and Human Health: Environmental Exposures and Biomarkers*, ed. M. I. Ahmad, M. Mahamood, M. Javed, and S. S. Alhewairini, Springer Nature Singapore, Singapore, 2023, pp. 55–74, DOI: 10.1007/978-981-99-2193-5_3.

4 X. Sun, Y. Zhao, J. Qiu and J. Xing, Review: alkali-activated blast furnace slag for eco-friendly binders, *J. Mater. Sci.*, 2022, **57**(3), 1599–1622, DOI: 10.1007/s10853-021-06682-8.

5 M. Elzeadani, D. V. Bompa and A. Y. Elghazouli, One part alkali activated materials: A state-of-the-art review Ordinary Portland cement, *J. Build. Eng.*, 2022, **57**, 104871, DOI: 10.1016/j.jobe.2022.104871.

6 J. L. Provis, Alkali-activated materials, *Cem. Concr. Res.*, 2018, **114**, 40–48, DOI: 10.1016/j.cemconres.2017.02.009.

7 D. Fisher, Sodium Hydroxide and Potassium Hydroxide,'' 2019. [Online]. Available: https://www.thesprucecrafts.com/sodium-hydroxide-vs-potassium-hydroxide-517051.

8 J. Fořt, M. Mildner and R. Černý, Consequences of omitting some important factors in the environmental analyses of commercial sodium silicate/sodium hydroxide use for alkaline activation in the light of comparison with cement-based composites, *Sci. Total Environ.*, 2024, **928**, 172324, DOI: 10.1016/j.scitotenv.2024.172324.

9 C. H. Baehr and W. Koehl, Soluble Silicates – Highly Versatile and Safe,'' in, *Int. J. Appl. Sci., SOFW J.*, 2007, **133**, 2–6.

10 National Organic Program, Sodium Silicate,'' 2025. [Online]. Available: https://www.ams.usda.gov/rules-regulations/organic/petitioned-substances%0ADocument.

11 S. Dall'Acqua, M. Fawer, R. Fritschi and C. Allenspach, Life cycle inventories for the production of detergent ingredients, *Int. J. Life Cycle Assess.*, 1999, **4**(4), 212, DOI: 10.1007/BF02979499.

12 A. M. Rashad, Y. Bai, P. A. M. Basheer, N. B. Milestone and N. C. Collier, Hydration and properties of sodium sulfate activated slag, *Cem. Concr. Compos.*, 2013, **37**(1), 20–29, DOI: 10.1016/j.cemconcomp.2012.12.010.

13 V. Ponomar, S. Kamali, T. Luukkonen, A. Hajimohammadi and K. Kilpimaa, The effect of gypsum on reaction kinetics and microstructure of alkali-activated CaO–FeO_x–SiO_2 slag, *Cem. Concr. Compos.*, 2025, **160**, DOI: 10.1016/j.cemconcomp.2025.106033.

14 Aakriti, S. Maiti, N. Jain and P. Prajapati, Synthesis of calcium sulfate whiskers via acidification exploiting FGD gypsum for improved binder properties, *Sustainable Chem. Pharm.*, 2024, **42**, 101745, DOI: 10.1016/j.scp.2024.101745.

15 Z. Yue, Y. Dhandapani, S. Adu-amankwah and S. A. Bernal, Phase evolution and performance of sodium sulfate-activated slag cement pastes, *Cement*, 2024, **18**, 100117, DOI: 10.1016/j.cement.2024.100117.

16 L. Li, A. Darquennes, K. Hannawi and C. Che, Effect of the Alkali-Sulphate Activators on the Hydration Process of Blast-Furnace Slag Mortars and Pastes, *Materials*, 2025, **18**(3), 514, DOI: 10.3390/ma18030514.

17 G. D. Schutter, X. Dai, S. Aydın, M. Y. Yardımcı and K. Lesage, Effect of $Ca(OH)_2$ Addition on the Engineering Properties of Sodium Sulfate Activated Slag, *Materials*, 2021, **14**, 4266, DOI: 10.3390/ma14154266 Academic.

18 S. Rubert, C. Angulski da Luz, M. V. F. Varela, J. I. Pereira Filho and R. D. Hooton, Hydration mechanisms of super-sulfated cement: The role of alkali activator and calcium sulfate content, *J. Therm. Anal. Calorim.*, 2018, **134**(2), 971–980, DOI: 10.1007/s10973-018-7243-6.

19 M. Ben Haha, B. Lothenbach, G. Le Saout and F. Winnefeld, Influence of slag chemistry on the hydration of alkali-activated blast-furnace slag - Part I: Effect of MgO, *Cem. Concr. Res.*, 2011, **41**(9), 955–963, DOI: 10.1016/j.cemconres.2011.05.002.

20 J. A. Tchio, E. Adesanya, B. Walkey and J. Yliniemi, Reaction kinetics of Na_2CO_3-activated blast furnace slag with organic ligands: insights from electrical conductivity measurements, *Cem. Concr. Compos.*, 2025, **29**(723–731), 1–11, DOI: 10.1016/j.cemconcomp.2025.106021.

21 R. Ramaswamy, M. Illikainen and J. Yliniemi, Influence of ligands as chemical admixtures in the early hydration of sodium carbonate-activated blast furnace slag, *Constr. Build. Mater.*, 2024, **422**(2), 135753, DOI: 10.1016/j.conbuildmat.2024.135753.

22 S. Bagheri, O. Mankinen, S. Ojala, V. Telkki, T. Luukkonen and J. Yliniemi, 3, 4-dihydroxybenzoic acid forms soluble complexes in cementitious systems, *J. Non. Cryst. Solids*, 2024, **633**(11), DOI: 10.1016/j.jnoncrysol.2024.122962.

23 Y. Wang, J. Chang, L. Yue, D. Zhou, Y. Liu, H. Wang, S. Yang and S. Cui, Effect of chelating solubilization via different alkanolamines on the dissolution properties of steel slag, *J. Cleaner Prod.*, 2022, **365**(4), 1–14, DOI: 10.1016/j.jclepro.2022.132824.

24 J. Chen, J. Jia, M. Zhu and L. Zhang, Advances of alkanolamine in hydration of Portland cement, *Mater. Today Commun.*, 2023, **37**(2), 107129, DOI: 10.1016/j.mtcomm.2023.107129.

25 T. Zhang, B. Ma, H. Tan, X. Liu, P. Chen and Z. Luo, Effect of TIPA on mechanical properties and hydration properties of cement-lithium slag system, *J. Environ. Manage.*, 2020, **276**(2), 111274, DOI: 10.1016/j.jenvman.2020.111274.

26 J. A. Tchio, E. Adesanya, R. Sliz, B. Walkley and J. Yliniemi, Electrochemical analysis of EAF slag-cement hydration and role of TIPA and glycine, *J. Mater. Sci. Mater. Eng.*, 2026, **3**, 1–19.

27 S. U. I. Chun, L. I. Yue and D. Qingjun, Hydration Process of Cement-Based Materials by AC Impedance Method, *J. Wuhan Univ. Technol., Mater. Sci. Ed.*, 2024, **30**(1), 142–146, DOI: 10.1007/s11595-015-1115-8.

28 A. F. Sosa Gallardo and J. L. Provis, Early-age characterisation of Portland cement by impedance spectroscopy, *Adv. Cem. Res.*, 2022, **34**(12), 542–559, DOI: 10.1680/jadcr.21.00103.

29 X. Hu, C. Shi, X. Liu, J. Zhang and G. D. Schutter, A review on microstructural characterization of cement-based materials by AC impedance spectroscopy, *Cem. Concr. Compos.*, 2019, **100**(4), 1–14, DOI: 10.1016/j.cemconcomp.2019.03.018.

30 L. Chi, W. Li, Z. Li, Z. Wang, S. Lu and Q. Liu, Investigation of the hydration properties of cement with EDTA by alternative current impedance spectroscopy, *Cem. Concr. Compos.*, 2022, **126**(8), 1–11, DOI: 10.1016/j.cemconcomp.2021.104365.

31 L. Chi, Z. Wang, S. Lu, H. Wang, K. Liu and W. Liu, Electrochimica Acta Early assessment of hydration and microstructure evolution of belite-calcium sulfoaluminate cement pastes by electrical impedance spectroscopy, *Electrochim. Acta*, 2021, **389**, 138699, DOI: 10.1016/j.electacta.2021.138699.

32 B. S. Krumgalz, Temperature Dependence of Mineral Solubility in Water. Part 3. Alkaline and Alkaline Earth Sulfates, *J. Phys. Chem. Ref. Data*, 2018, **47**(2), DOI: 10.1063/1.5031951.

33 A. F. Sosa Gallardo and J. L. Provis, Electrochemical cell design and impedance spectroscopy of cement hydration, *J. Mater. Sci.*, 2021, **56**(2), 1203–1220, DOI: 10.1007/s10853-020-05397-6.

34 R. Masoudi and R. D. Hooton, Examining the hydration mechanism of supersulfated cements made with high and low-alumina slags, *Cem. Concr. Compos.*, 2019, **103**, 193–203, DOI: 10.1016/j.cemconcomp.2019.05.001.

35 D. Lowke and C. Gehlen, The zeta potential of cement and additions in cementitious suspensions with high solid fraction, *Cem. Concr. Res.*, 2017, **95**, 195–204, DOI: 10.1016/j.cemconres.2017.02.016.

36 L. Ferrari, J. Kaufmann, F. Winnefeld and J. Plank, Interaction of cement model systems with superplasticizers investigated by atomic force microscopy, zeta potential, and adsorption measurements, *J. Colloid Interface Sci.*, 2010, **347**(1), 15–24, DOI: 10.1016/j.jcis.2010.03.005.
37 D. Lowke and C. Gehlen, *SP-302: Effect of pore solution composition on zeta potential and superplasticizer adsorption*, Am. Concr. Institute, ACI Spec. Publ., 2015, vol. 2, no. SP 302, pp. 253–264, DOI: 10.14359/51688099.
38 Emerson process Management, '''Conductance Data For Commonly Used Chemicals,''' 44-6039/rev. B, 2010. [Online]. Available: https://www.raihome.com.
39 Q. Zhai and K. Kurumisawa, Effects of cation in sulfate chloride and nitrite on $Ca(OH)_2$ activated ground granulated blast-furnace slag, *Cem. Concr. Compos.*, 2022, **133**, 104648, DOI: 10.1016/j.cemconcomp.2022.104648.
40 J. L. P. S. A. Bernal, X. Xinyuan and O. H. Hussein, ''International RILEM Conference Materials, Systems and Structures in Civil Engineering 2016 – Segment on Concrete with Supplementary Cementitious Materials Lyngby, Denmark, August 22-24, 2016,'' in ISBN 978-2-35158-180-3, e-ISBN 978-2-35158-181-0, Denmark, 2016, pp. 299–307. [Online]. Available: https://eprints.whiterose.ac.uk/104315/.
41 T. Zhang, B. Ma, H. Tan, X. Liu, P. Chen and Z. Luo, Effect of TIPA on mechanical properties and hydration properties of cement-lithium slag system, *J. Environ. Manage.*, 2020, **276**, DOI: 10.1016/j.jenvman.2020.111274.